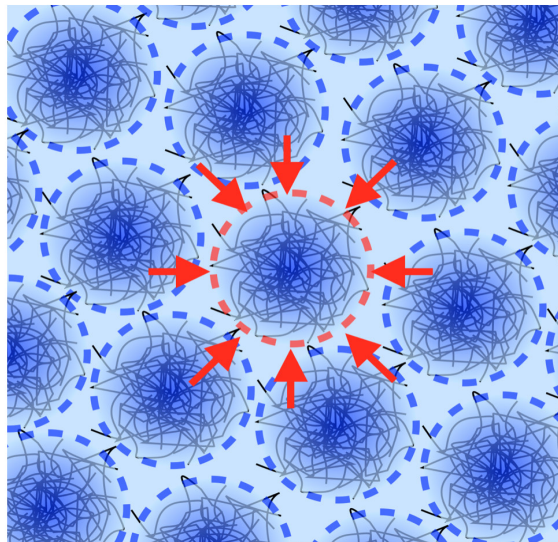
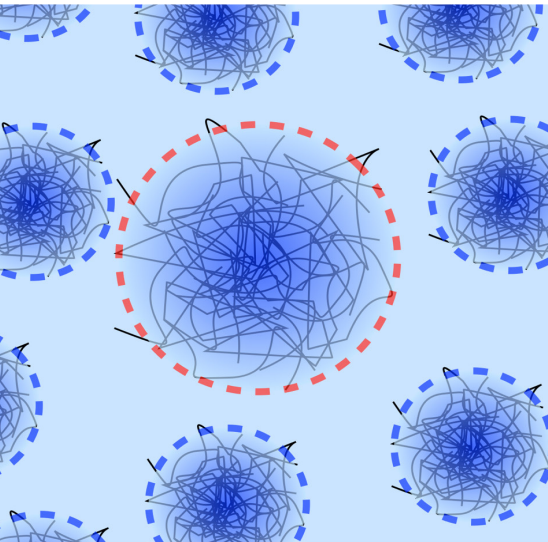



Number 50 | October 2017

SWISS NEUTRON NEWS



Schweizerische Gesellschaft für Neutronenstreuung
Société Suisse pour la Diffusion des Neutrons
Swiss Neutron Scattering Society



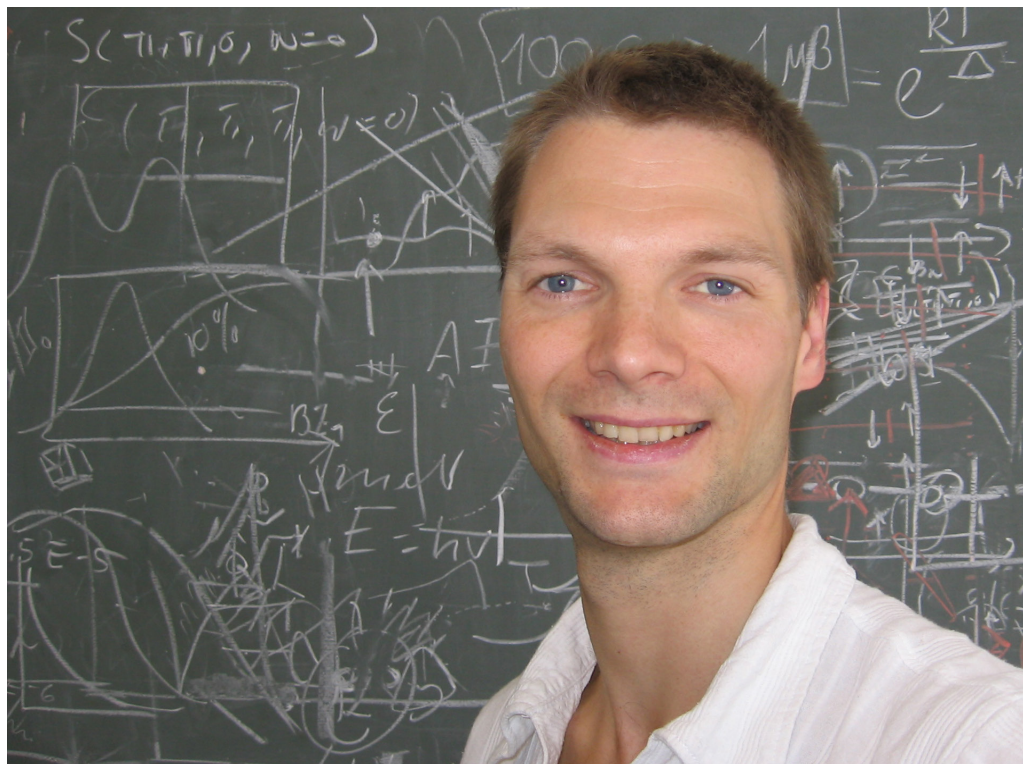
On the cover

Sketch of the self-healing behavior of pNIPAM microgel suspensions. See the related article “Small-angle neutron scattering to unravel the selective deswelling of microgel particles” by A. Scotti et al.

Contents

- 4** The President's Page
- 6** The European Neutron Source Landscape
- 14** Small-angle neutron scattering to unravel the selective deswelling of microgel particles
- 22** Announcements
- 23** Conferences and Workshops
- 27** Editorial

The President's Page



Dear Colleagues,

Welcome to this issue of neutron news.

Let me start by a big congratulations to Dr Viviane Lutz-Bueno, who received the 2017 Young Scientist Prize of the Swiss Neutron Scattering Society for her thesis work on mi-

cellar aggregates and their behavior under confinement and flow, using a combination of both small-angle neutron and X-ray scattering experiments. This prize is kindly sponsored by SwissNeutronics.

In this context, I would also like to thank the members of the prize committee. Again this



year, an impressive field of promising young scientists had been nominated.

Not only is SINQ celebrating its 20th year anniversary this year - which was the occasion of a very nice event at PSI. This year is also the 25th anniversary of our Swiss Neutron Scattering Society. It is inspiring how the field

continues to produce excellent new scientists. In this issue you will find an article by Kurt Clausen reporting partly on the history of neutron facilities, and very timely on the evolution of the European neutron scattering landscape. It is clear that we have challenges ahead of us. Neutron science is far from the situation of X-rays, where almost every country contributes a synchrotron. It is therefore vital that we continue a productive sharing in provision and utilization of neutron scattering. This summer many of us enjoyed an inspiring International Conference for Neutron Scattering (ICNS) in Daejeon, South Korea. I would like to thank the organizers for a well planned and executed conference, as well as an interesting visit to the Hanaro reactor. This visit reminded us how successfully operating neutron sources is not just a technical but also administrative challenge. It is greatly saddening to see multiple neutron scattering reactors technically operational paused for other reasons, such as Hanaro in South Korea, CAR in China and JRR3 in Japan, and very unfortunately for the rest of 2017 ILL was recently added to this list. Please join me in crossing our fingers and sending our wishes that these facilities may succeed in solving technical and administrative hurdles to again produce wonderful science.

Cordially,
Henrik M. Ronnow

The European Neutron Source Landscape

Prof. Kurt Nørgaard Clausen

Paul Scherrer Institut &

The Technical University of Denmark

On the occasion of my retirement from 40 years of service to neutron scattering in Europe – the last 13 in Switzerland, SGN asked me to write an article on “the past and the future of the European neutron landscape”. This is a huge topic and a comprehensive view will be beyond the scope of a short article. In this article, I have chosen to bring my personal view on the development of the neutron Landscape in Europe and what I consider as important developments and milestones.

The end of the Second World War (WWII) had shown the devastating power of the nuclear chain reaction but also raised very high hopes for peaceful use of nuclear technology as a means to rebuild and develop a prosperous society from the ruins. The first reactors or “piles” where you could get access to thermal neutron beams were constructed in the US during WWII and the first outside the US in Canada just after the war. The very early demonstration of Neutron Diffraction (Clifford Glenwood Shull, X-10 Oak Ridge ~1946) and Spectroscopy (Bertram Brockhouse, NRX reactor Chalk River ~1955) were thus made in America (See Fig. 1). For these discoveries Shull and Brockhouse were awarded the 1994 Nobel Prize in Physics.

In almost all European countries, small nuclear reactors – often called materials testing reactors – were built to develop the Euro-

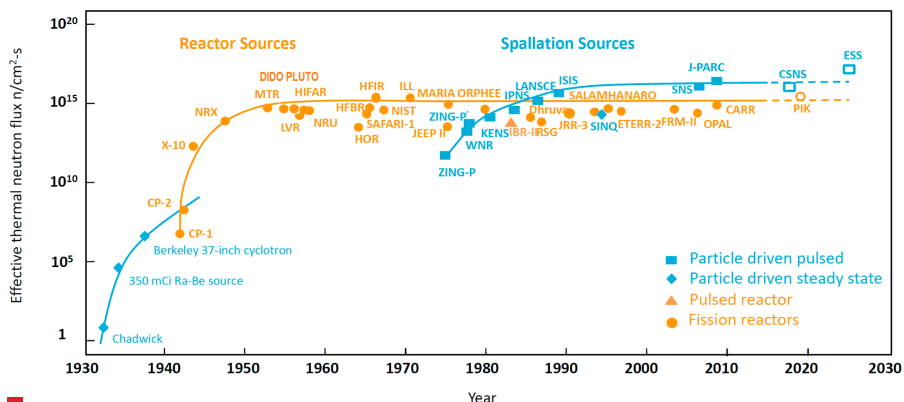


Figure 1

Effective thermal neutron flux of neutron sources versus year of first operation, updated from *Neutron Scattering* by K. Sköld and D.L. Price, eds., Academic Press 1986.

pean nuclear competence. The key drivers for this development were in most cases a mixture of securing a source of cheap, abundant energy and developing nuclear technologies for other peaceful uses. The cold war meant that in some cases or at some level military aspects probably also played a role. These facilities were however built without having neutron scattering in mind.

The UK DIDO(1956)/PLUTO(1957) materials testing reactor design allowed for power levels up to 25 MW and had respectively radial and tangential beam tubes close to a core of highly enriched Uranium and very importantly both were cooled and moderated with heavy water. These reactors were excellently suited for neutron scattering. DIDO type reactors were shortly after built at Jülich in Germany and Lukas Heights in Australia and a PLUTO type reactor in Denmark. In the sixties, Europe with especially Harwell in the UK took a lead-

ing role in the development of neutron sources, instrumentation and scattering. Most of these early Materials Testing reactors have now been closed, and often replaced by modern medium flux reactors designed with neutron scattering as a priority use (Orphee at Sacclay, FRM-II at MLZ in Munich, BER-II at HZB in Berlin).

The next major step forward was the development of high flux sources dedicated to neutron scattering. This development started in the US with HFBR – the High Flux Beam Reactor at Brookhaven. The true revolution however happened in Europe with the ILL start-up in 1972 using novel technology (especially extensive use of neutron guides) and last but not least operating with a formalised neutron user programme.

In a nuclear reactor, each produced free neutron is associated with a release of 180 MeV from the fission process and each neu-

Process	Example	Yield	Energy deposition in target (MeV/n)	Average Kinetic Energy carried away by neutron (MeV/n)
Fission	^{235}U	1 n/fission	180	2
Spallation	1.3 GeV protons on Hg	33 - 40 n/proton	30 - 35	2 – 5
Fusion DT solid target	400 keV Deuterons on T in titanium	$4.0 \cdot 10^{-5}$ n/D	10'000	14.1
Fusion DT inertial confinement	D + T fusion in laser or ion-beam imploded target	1 n/fusion	3.5 ± 0.1	14.1

Table 1

Processes for release of free neutrons, the associated yield, and energy deposited in the target and carried away by the released neutron.

tron carries away an average kinetic energy of ca. 2 MeV (See table 1). This energy is converted into heat, and it is the mechanical stability and ability to remove this heat from the fuel elements that provides the most stringent limit to the neutron flux in the core of a reactor. This limit has been reached by the ILL, fluxes substantially beyond that of the ILL would neither be viable from an economic nor from a safety point of view. With accelerator driven spallation neutron sources, neutrons can be extracted with less energy release per useful neutron (see table 1) and in addi-

tion be produced in pulses with much higher peak fluxes than in a reactor, both these effects are key to secure the next major step in neutron source performance. Developing Spallation neutron sources were again pioneered globally, IPNS at Argonne US, KEK Japan and in Europe: FZ-Jülich in Germany, Harwell/ISIS in the UK now operating the pulsed spallation source ISIS, and PSI in Switzerland now operating the continuous spallation source SINQ.

ILL, ISIS and the modern European continuous sources MLZ, LLB, SINQ, HZB with well



Figure 2

The European landscape for neutron scattering facilities operating a user programme and ESS which is under construction and expecting first users in 2023.

organised user access programmes and a wide range of instrument specialisation/capability, form the backbone of the current European neutron eco system (see figure 2),

with sufficient quality and quantity to sustain the very diverse European User community. This combination is unique worldwide and has secured European supremacy in this ex-

perimental field for more than 50 years. At the outset of the open user-programmes in the early seventies, the user community was mainly from physics and structural chemistry and professional users. With the development of better user interfaces, new instrumentation, and sample environments, the user base has broadened in different ways. The number of casual users (one or fewer experiments per year) and of scientific fields using neutrons has increased dramatically. Today engineering, soft matter and life science are bigger users than physics, and the higher the performance of the source, the higher the share of life science.

The non European neutron landscape is currently being strengthened with MW class spallation neutron sources in the US and Japan, a new reactor source in Australia, construction of a new spallation neutron source in China and a research reactor in Argentina. In Europe, the situation is dramatically different: several key reactor-based neutron sources will be permanently closed down in the next years due to national decisions, while the European Spallation Source (ESS) in Lund will be fully operative only in the mid or late 2020s. ESFRI – The European Strategy Forum for Research Infrastructure, found it necessary to analyse at the appropriate level the implications in terms of capacity and capability of neutron science in Europe, both during the crossover period of national reactors with the ESS, and in the longer term and, in 2014, created a Neutron Landscape Group (NLG). The report from this group can be found on the ESFRI home page using the following link: http://www.esfri.eu/sites/default/files/u4/NGL_CombinedReport_300616_1515%20%281%29.pdf

One of the key first issues the NLG had to deal with was how to quantify the output from the facilities with very different flux, number of instruments, specialization/usage of the facilities etc. The best data for this was provided by the ILL associates, who annually provide a statistics of scientific output in terms of high quality publications, i.e. publications in a selection of publications with a high impact factor (See figure 3).

Because of well developed and organised user programmes, scientists in general have access to all facilities (and use this capability) and therefore in general perform their experiments at the overall most appropriate facility. Some experiments are only feasible with access to the highest flux, others need specialised instrumentation, local scientific specialisation or sample environment (in situ, in operando etc.) – a sizeable fraction of publications therefore contain data from more than one facility. In addition there is an overall need for method development, training, fast access etc., which often are better suited for the smaller facilities.

All the facilities in Figure 3 are sufficiently funded to operate a scientific programme, have an updated suite of instruments and infrastructure, sustain a user programme, and have a strategy and role that fits into the overall neutron scattering landscape. In this case, it can be seen that the output is more or less given by the number of beam-lines/instruments in user operation and that the actual flux has less impact in the current neutron eco-system. Loosing either the high flux facilities or the specialisation from the medium flux facilities would, however, both lead to a break-down of the field – the eco-system – in the long term.

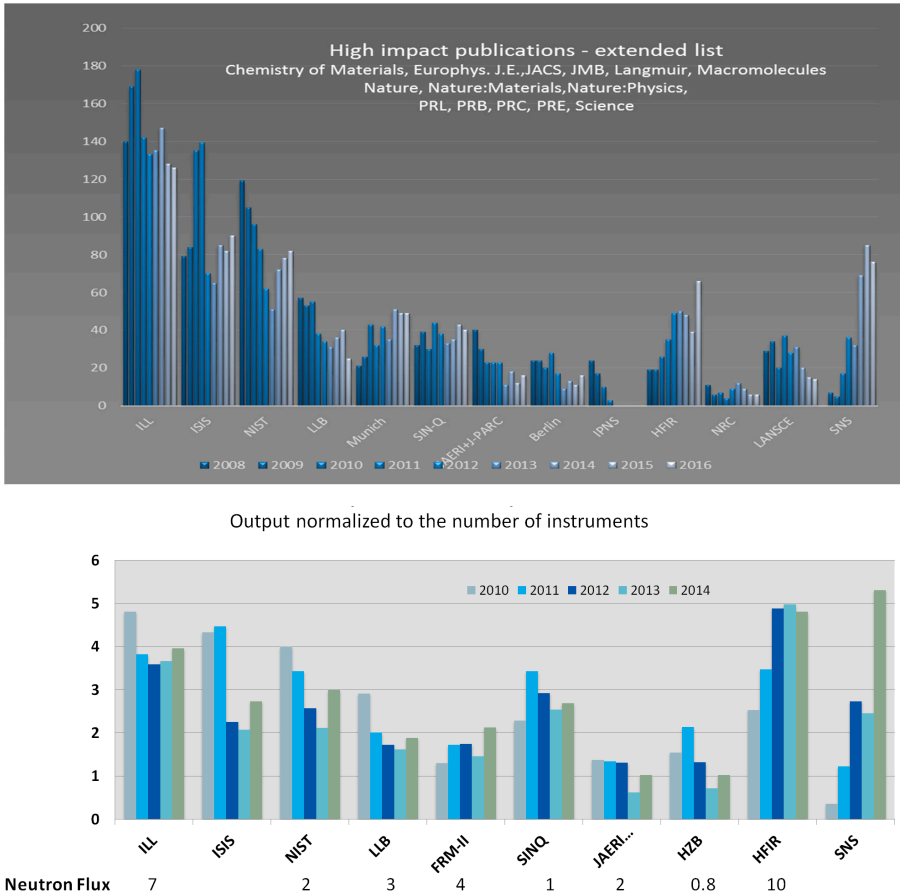


Figure 3

Top: Scientific output from a selection of the most important neutron sources worldwide – Source ILL Library, ILL Associates reports. **Bottom:** A selection of the data from the top normalised to the number of instruments on the given facility. At the very bottom, the approximate relative flux of the continuous facilities are listed – Graph prepared by Christian Rüegg (PSI) and Helmut Schober (ILL).

Another lesson from Figure 3 is that, dated from a major upgrade or start of a new facility, it takes about 5 to 7 years before full capacity

is reached. (The same has been found for ILL, ISIS, SINQ and other similar complex Large Scale Facilities).

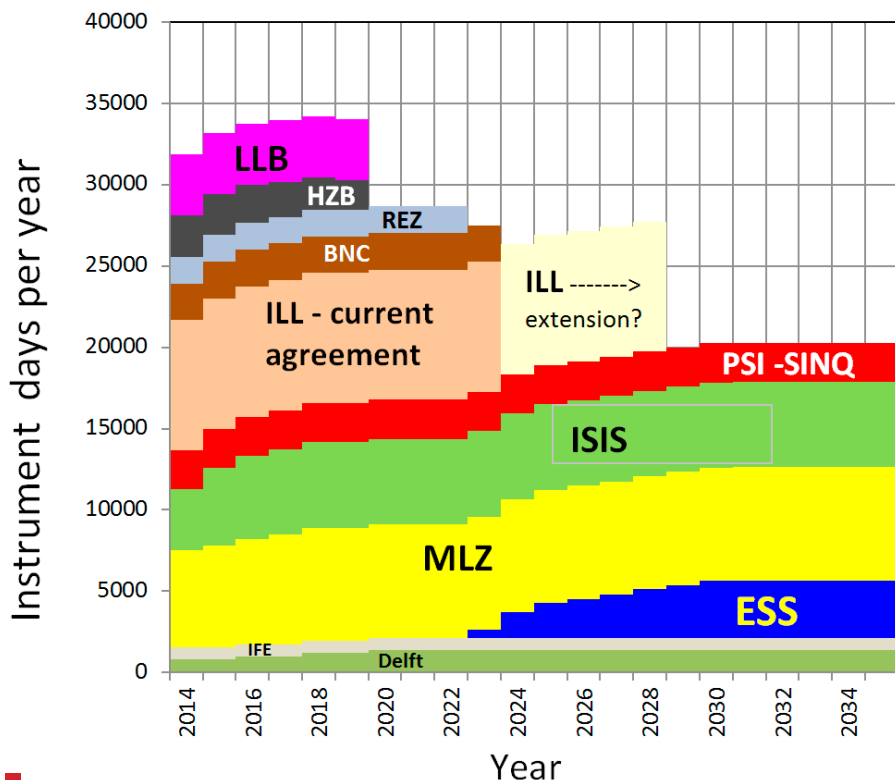


Figure 4

Available neutron instrument days for neutron users based on data from the different facility directors in 2014 (ESS data updated 2017). Source: the ESFRI Neutron Landscape Report http://www.esfri.eu/sites/default/files/u4/NGL_CombinedReport_300616_1515%20%281%29.pdf.

In the NLG, we therefore concluded that the best way to quantify access and the size of user community that the overall system of well run and funded neutron scattering facilities can sustain is best described by the available instrument days in user mode.

In order to obtain up-to-date statistics concerning individual source operations, the

Neutron Landscape Group asked each neutron facility head in Europe to complete a detailed questionnaire. We provided guidance to the sources on definitions (e.g. what constitutes a “day for science”) and, apart from a few clarifying queries, we have accepted the responses as presented to us. The data in Figure 4 represents a snap-shot of the situation in

2014 and the known future funding situation, upgrading scenarios, life time etc. at that time. We are well aware that there are small inconsistencies, but we have taken the view that the uncertainties in the data and the inconsistencies are of the same order. We are more interested in the overall global scenario than in details. The data was collected during the summer of 2014 and has not been adjusted for recent developments at ILL, BER-II or LLB or the SINQ upgrade in 2019, which have in the interim already signalled a fall in beam days. To counteract this, operational funding for ISIS has improved somewhat.

In Figure 4, the largest contribution comes from the ILL with more than 40 available beamports. The, ESS is, in this graph, limited to 22 instruments, but could, if funding was available, increase to a similar number of instruments beyond 2030. However, a couple of new instruments per year is the fastest realistic growth rate with an operating facility.

An additional lesson from the NLG study was that building additional neutron sources with an impact before 2035 would not be realistic and that building ESS in Europe will exploit most of the relevant available European competence, i.e. that access to neutrons would have to be predominantly provided by the operating European facilities and only to a limited extent by overseas facilities.

From Figure 4, it is very clear that Europe faces a huge challenge in terms of being able to sustain its user community. It will be a very different neutron-eco system with one big high flux facility and only very few smaller facilities – i.e. new ideas for user operation, access modes, funding schemes etc. must be developed. It is also abundantly clear that SINQ has

a key role to play. This and the extension of the operational period of ILL beyond the current convention for ILL as well as a timely start of ESS are essential. Exciting times are ahead of us – the SINQ guide upgrade and the ESS will lead to entirely new capabilities that will allow for new science and will also change the composition of the user community.

Small-angle neutron scattering to unravel the selective deswelling of microgel particles

A. Scotti ^{1,2,3}, U. Gasser ¹, L. A. Lyon ⁴, and A. Fernandez-Nieves ²

¹Laboratory for Neutron Scattering and Imaging, Paul Scherrer Institut, 5232 Villigen, Switzerland

²School of Physics, Georgia Institute of Technology, Atlanta, USA

³current address: Institute of Physical Chemistry, RWTH Aachen University, 52056 Aachen, Germany

⁴Chapman University, Schmid College of Science and Technology, Orange, CA, USA

Dated: August 29, 2017

For soft, compressible particles, the role of polydispersity in crystallization is fundamentally changed compared to hard, incompressible spheres. In this paper, we describe the fundamental role played by Small-Angle Neutron Scattering (SANS) in understanding selective particle deswelling in concentrated suspensions of microgel particles. Using SANS, we directly measure the single particle form factor in concentrated suspensions and quantify how individual particles deswell. Interestingly, we find that the particle size depends on the suspension osmotic pressure. Once the osmotic pressure of the suspension exceeds the bulk modulus of the microgel particles, deswelling occurs; this happens first to the softest particles, which also are the largest. As a result, suspension polydispersity spontaneously decreases allowing for crystallization in instances where this would otherwise not happen.

Small-angle neutron scattering (SANS) is a perfect experimental tool to study soft condensed matter for two principal reasons: First, the sizes of the relevant structures are in the range between tens and thousands of nanometers. Second, the scattering contrast can be tuned by “labeling” parts of interest of the sample with a chosen isotope of a chemical element occurring in the sample. The most important option is to substitute Hydrogen with Deuterium. Since the scattering length for these two elements are $b_H = -3.7406 \cdot 10^{-15} \text{ m}$ and $b_D = 6.671 \cdot 10^{-15} \text{ m}$, SANS can clearly distinguish between these two isotopes, in contrast to small-angle X-ray scattering. If we are interested in the size and internal structure of a single colloidal particle, for instance because it is soft, in a concentrated suspension, we want to obtain the form factor, $P(q)$, ideally without having to deal with the structure of the colloidal suspension, which is given by the structure factor, $S(q)$, in the scattering intensity $I(q) = P(q)S(q)$, which is obtained in a SANS measurement. Direct form factor measurements can be done by mixing a majority of deuterated particles with a few protonated ones, as illustrated by the red and green particles in Fig. 1A. For a direct measurement of the form factor, the scattering contrast between the deuterated particles and the solvent can be reduced to zero such that the few protonated particles dominate the scattered signal $I(q)$ (Fig. 1B). The few proto-

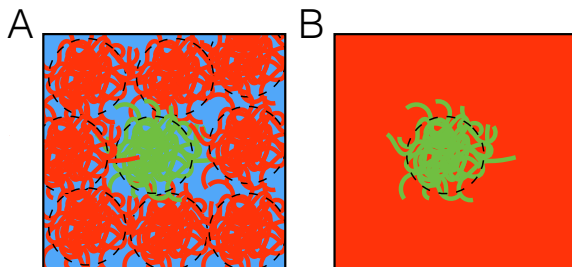


Figure 1

(A) Mixture of deuterated (red) and protonated (green) particles in a solvent (light blue). (B) The same mixture of deuterated and protonated particles in a solvent with the scattering length density equal to the one of the deuterated particles. As a consequence, the protonated particles are invisible.

nated particles act as tracer particles with $S(q)=1$ such that the form factor can directly be measured [1, 2]. For our microgel particles, the scattering length density of the deuterated particles is matched by choosing the proper mixture of heavy water, D_2O , and light water, H_2O , as solvent.

We have used this technique to investigate the behavior of pNIPAM microgel particles, which are crosslinked, polymeric networks immersed in a solvent, usually water. pNIPAM microgels exist in a swollen state below and in a collapsed, deswollen state above 32°C , as the solvent quality changes at this critical temperature. In the following, temperature is, however, limited to the range $18^\circ\text{C} < T < 20^\circ\text{C}$ where the particles are fully swollen. The deswelling discussed here happens at high concentrations of the microgel suspension at a fixed temperature. Due to their compressibility, large microgels surrounded by a majority of small but otherwise identical microgels can deswell and fit in the structure, e.g. a

nated particles act as tracer particles with $S(q)=1$ such that the form factor can directly be measured [1, 2]. For our microgel particles, the scattering length density of the deuterated particles is matched by choosing the proper mixture of heavy water, D_2O , and light water, H_2O , as solvent.

We have used this technique to investigate the behavior of pNIPAM microgel particles, which are crosslinked, polymeric networks immersed in a solvent, usually water. pNIPAM microgels exist in a swollen state below and in a collapsed, deswollen state above 32°C , as the solvent quality changes at this critical temperature. In the following, temperature is, however, limited to the range $18^\circ\text{C} < T < 20^\circ\text{C}$ where the particles are fully swollen. The deswelling discussed here happens at high concentrations of the microgel suspension at a fixed temperature. Due to their compressibility, large microgels surrounded by a majority of small but otherwise identical microgels can deswell and fit in the structure, e.g. a

crystal lattice, formed by the small ones [3]. This allows for crystallization without any defects created by the large particles, which, under dilute conditions, are too large to fit in the crystal lattice. Microgel deswelling is also observed in monodisperse suspensions at high concentrations [4–7]. This spontaneous particle deswelling with reduction of polydispersity has not been observed in any other material and completely changes the role of size polydispersity for crystallization compared to incompressible, hard spheres [8]. In our recent work, we have shown how this mechanism is triggered by the increase in osmotic pressure due to counterion clouds surrounding the particles. Although pNIPAM is an uncharged polymer, pNIPAM microgels carry charged groups on their periphery, which originate from the initiator employed in their synthesis [1]. These counterion clouds define the swelling behavior at high concentrations when counterion clouds overlap, and they are also of great importance to understand the phase behavior of pNIPAM suspensions. In contrast to hard spheres, where crystallization is suppressed when the size polydispersity is higher than 12% [9–11], the deswelling mechanism in microgels allows suspensions of these soft, compressible particles to crystallize even if the size polydispersity is as high as 18.5% [8]. In this article, we examine the central role of SANS with contrast variation for the aforementioned study.

We synthesize two kinds of soft, deformable particles using precipitation polymerization: Protonated and deuterated poly-N-isopropylacrylamide (pNIPAM) based microgels. For the synthesis of the former, the solvent (distilled, deionized water), NIPAM ($C_6H_{11}NO$),

the cross-linker N,N'-methylene-bis(acrylamide) (BIS, $C_7H_{10}N_2O_2$) [12], and the surfactant sodium dodecyl sulfate (SDS, $CH_3(CH_2)_{11}OSO_3Na$) were mixed together in a reactor. Proper tuning of the relative concentration of crosslinker and NIPAM monomer allows obtaining a final swollen size. The surfactant is needed to control the deswollen size [13]. The deuterated particles were obtained by substituting the NIPAM monomer ($C_6H_{11}NO$) with D_7 -NIPAM ($C_6D_7H_4NO$) and following essentially the same synthesis procedures described above. After the synthesis, all the samples were freeze dried. The powder was then redispersed in H_2O and/or D_2O to obtain suspensions at the desired concentration and scattering contrast.

The hydrodynamic radii of the protonated, $R_H = (182 \pm 2)$ nm, and deuterated particles, $R_D = (117 \pm 7)$ nm, were determined by dynamic light scattering using a LS-Instruments 3D DLS-Pro spectrometer. All measurements were taken in water with the particles in the fully swollen state at a temperature $T = (20.0 \pm 0.5)^\circ C$. Performing both Cumulants analysis [14] and a modified CONTIN analysis [15] we obtained the radii given above and polydispersities equal to $(9.8 \pm 2.5)\%$ and $(21 \pm 3)\%$ for the protonated and deuterated particles, respectively.

The scattering length density of the deuterated particles has to be determined to contrast match them with the correct mixture of H_2O and D_2O . For this purpose, we performed SANS measurements at low momentum transfer, q , in the Guinier regime, where $I(q) = n_p \Delta\rho^2 \langle V_p^2 \rangle \exp[-(q^2 R_g^2)/3]$ [16], with R_g the radius of gyration, $\Delta\rho$ the scattering-length-density contrast between the sol-

vent and the deuterated particles, and n_p the number density of particles. Dilute suspensions of the deuterated microgels in different mixtures of light and heavy water (0, 28, 56, 96, and 100 wt% D₂O) were used to vary $\Delta\rho$ and to find the mixture matching the deuterated particles. With dilute samples, we can neglect the structure factor, $S(q)$, of the microgel suspension and thus:

$$\lim_{q \rightarrow 0} I(q) = n_p \Delta\rho^2 \langle V_p^2 \rangle. \quad (1)$$

where the limit $\lim_{q \rightarrow 0} I(q)$ is obtained by extrapolation of the SANS measurement in the Guinier regime. For our microgels, this is the configuration for the lowest accessible momentum transfers, q . In the very low- q region, $I(q)$ is found to decrease linearly with q^2 , as expected from Eq.1. As the ratio of n_p from one sample to the other is known and $\langle V_p^2 \rangle$ is obtained from the same form factor measurement, we determine $\Delta\rho^2$ using equation 1 for each heavy/light water mixture. From here, we find that the match point for the deuterated particles corresponds to a mixture of 83 wt% D₂O and 17 wt% H₂O [1].

Once we know the solvent composition that contrast matches the deuterated microgels, we prepare samples at different concentrations comprised of a majority of deuterated particles and $n_H = 2.9\%$ protonated microgels, where $n_H = N_H / (N_H + N_D)$, with N_H and N_D the number of protonated and deuterated particles in suspension. As microgels deform, shrink, and/or interpenetrate at high concentrations, the concentration of a microgel suspension is not directly related to the common volume fraction, ϕ , but with the generalized volume fraction, ζ , which is defined as the

volume occupied by the swollen particles in dilute conditions, relative to the available volume. While ϕ is limited to values ≤ 1 , ζ can increase beyond 1, when particles are forced to shrink or interpenetrate. Note that ζ is linked to the weight concentration, c , by a conversion constant: $\zeta = kc$, where k contains information about the relative density of the polymer and the solvent and the ratio between the swollen and collapsed radii of the microgel. Viscosimetry and the Stokes-Einstein relation allow obtaining the value of k [1, 4]. We measured the relative viscosity of 6 samples with concentrations between 0.1 and 0.4 wt% and fitted the data using the Einstein-Batchelor equation $\eta_r = 1 + 2.5\zeta + 5.9\zeta^2 = 1 + 2.5kc + 5.9(kc)^2$ [17]. From here, we can obtain the conversion constants for the deuterated and protonated particles, $k_D = 17.5 \pm 0.2$ and $k_H = 18.49 \pm 0.07$, respectively. Knowing these constants, the generalized volume fractions of the deuterated and protonated particles, ζ_D and ζ_H respectively, are computed from their weight concentrations c_D and c_H : $\zeta_D = k_D c_D$ and $\zeta_H = k_H c_H$. Since the total volume in ζ_D and ζ_H is the same, the total volume fraction of the samples is simply $\zeta = \zeta_D + \zeta_H$.

SANS experiments were performed using two different instruments: SANS-I and SANS-II at SINQ, Paul Scherrer Institut, Villigen Switzerland. On SANS-I, we have covered the q -range of interest using two configurations: sample detector distance, $d_{sd} = 18$ m with wavelength $\lambda = 0.8$ nm and $d_{sd} = 4.5$ m with $\lambda = 0.8$ nm. On SANS-II, we also used two configurations: $d_{sd} = 6$ m with $\lambda = 1.054$ nm and $d_{sd} = 3$ m with $\lambda = 0.53$ nm. Both SANS-I and SANS-II are equipped with a ³He detector with

128 × 128 pixels and pixel sizes of 7.5 mm and 4.3 mm, respectively. The temperature was set to (18.0 ± 0.5)°C in all SANS measurements.

Samples were realized with the H₂O / D₂O solvent matching the deuterated microgels, as given above, for direct form factor measurements at all sample concentrations. With this scattering contrast, the small fraction of protonated microgels in the suspension dominates the scattering intensity such that the structure factor, $S(q)$, in the scattered intensity, $I(q) = P(q)S(q)$, can be neglected. We covered a ζ -range between 0.22 ± 0.01 and 1.21 ± 0.02 to obtain form factors from dilute up to overpacked conditions. The form factor is given by the overall shape as well as the internal structure of a microgel. The data are fitted using a model describing a “fuzzy-sphere” [18], consisting of a compact core with radius R_{core} , surrounded by a shell with decreasing density. Mathematically, the microgel structure results from convoluting the model for a homogenous sphere with radius R_{core} , and a Gaussian with standard deviation σ_s . In reciprocal space, the convolution becomes a multiplication, and we obtain the following form factor model:

$$P_1(q) = \left[\frac{3(\sin qR_{\text{core}} - qR_{\text{core}} \cos qR_{\text{core}})}{(qR_{\text{core}})^3} e^{-\frac{(\sigma_s q)^2}{2}} \right]^2 \quad (2)$$

The size polydispersity of the microgel particles is taken into account as polydispersity in the core using a Gaussian size distribution with standard deviation $\sigma_p R_{\text{core}}^{\text{av}}$:

$$D(R_{\text{core}}) = \frac{1}{\sqrt{2\pi}\sigma_p R_{\text{core}}^{\text{av}}} e^{-\frac{(R_{\text{core}} - R_{\text{core}}^{\text{av}})^2}{2(\sigma_p R_{\text{core}}^{\text{av}})^2}}, \quad (3)$$

where $R_{\text{core}}^{\text{av}}$ and σ_p are the mean core radius and the core polydispersity, respectively. Due

to the Gaussian in Eq. 2, the spherical core only dominates at low momentum transfer, while for $q \gg \pi/\sigma$, SANS probes the inhomogeneities inside the microgels. This contribution to the form factor is considered by adding a Lorentzian term [19], $I_{\text{chain}}(q) = I_{\text{chain}}(0)/[1 + (\xi q)^2]$, where ξ is related to the mesh size of the polymer in the particle, and $I_{\text{chain}}(0)$ is the zero- q intensity contribution due to the internal structure. The model for the form factor of a microgel particle becomes:

$$P(q) = \frac{1}{\langle V^2 \rangle} \int_0^\infty dR_{\text{core}} D(R_{\text{core}}) V^2(R_{\text{core}}) P_1(q) + I_{\text{chain}}(q) + B \quad (4)$$

with $\langle V^2 \rangle = \int_0^\infty dR_{\text{core}} V^2(R_{\text{core}}) D(R_{\text{core}})$, and $V(R_{\text{core}}) = 4\pi R_{\text{core}}^3/3$ the average squared core volume and the volume of the core, respectively. The constant B is added to account for incoherent scattering, which is mostly due to incoherent scattering from hydrogen contained in the solvent and the particles. The instrument resolution causes a smearing of the data. This is accounted for by convoluting $P(q)$ with a Gaussian [20]:

$$P_s(q) = \frac{1}{\sqrt{2\pi}\sigma_r} \int_0^\infty dq' e^{-\frac{(q-q')^2}{2\sigma_r^2}} P(q'), \quad (5)$$

where σ_r is the q -dependent standard deviation: $\sigma_r(q) \propto 1/\arcsin[(q\lambda)/(4\pi)]$. We have used Eqs. 4 and 5 to fit the small-angle scattering data and obtain the parameters R_{core} , σ_s , σ_p , $I_{\text{chain}}(0)$, ξ and B characterizing the size and internal structure of the microgels. The total particle radius is calculated as $R_{\text{SANS}} = R_{\text{core}} + 2\sigma_s$.

Fig. 2 shows two form factors of the large protonated particles. The faster decay of $P(q)$ at $\zeta \approx 1.2$ in panel B with respect the one at $\zeta \approx 0.22$ in panel A reveals that the particles deswell with increasing concentration. The

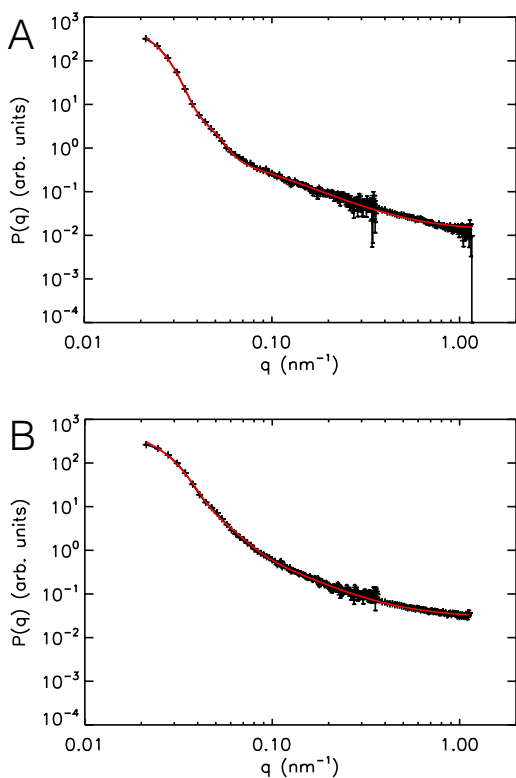


Figure 2

SANS form factors of the large protonated microgels (+) and corresponding fits (red line) in a bidisperse sample with $n_H = (2.9 \pm 0.3)\%$ and (A) $\zeta = 0.22 \pm 0.03$ and (B) $\zeta = 1.21 \pm 0.04$.

change in the decay is mainly caused by the compression of the fuzzy shell, the softest part of a microgel particle, which implies a decrease of σ_s . More examples of fitted data are presented in Ref. [1]; these also indicate that deswelling of the particles occurs as the particle concentration increases above a threshold value, and that it is the fuzzy shell what is first compressed, followed by the core.

SANS with contrast matching is the only technique allowing for the investigation of the single-particle structure in concentrated samples. For example, small-angle X-ray scattering (SAXS), another powerful method to probe soft matter, does not allow for contrast variation with deuterium and hydrogen, since their scattering length densities for X-rays are very close and, therefore, indistinguishable. The SAXS signal does not depend on the isotopes in the composition of the sample but is given by the electron density in the sample. Also, confocal microscopy, often used to probe colloidal systems, does not have the resolution to resolve the internal structure of single particles used in our study. Super-resolved microscopy might represent a fascinating option to investigate single microgels in real space but, at the best of our knowledge, the only studies published so far have only considered particles in dilute suspensions [21, 22]. Since we are interested in the changes of larger particles immersed in a sea of smaller ones, we chose to contrast match the majority of deuter-

ated particles instead of using SANS with zero average contrast (ZAC). This technique is another suitable contrast-matching method to study the single-particle form factor in concentrated samples [2, 23]. However, the mixtures of deuterated and protonated microgels for a ZAC study need to be very close in terms of size and internal structure, given by the polymer density and cross-linker concentra-

tion across the particle, to allow for measuring the wanted form factor. This was not the case of our study.

The mechanism of spontaneous particle deswelling presented in Ref. [1] has direct consequences for the phase behavior of soft, compressible microgels. Although the deswelling mechanism was studied with highly polydisperse and also suspensions with bimodal size distribution, the deswelling mechanism is also relevant for monodisperse suspensions and, therefore, is expected to be quite general for soft polymer particles. The role of polydispersity changes in a fundamental way compared to suspensions of rigid, hard spheres [8]. In Fig. 3A, a suspension of monodisperse, incompressible spheres at low concentration is sketched. With increasing concentration, between a volume fraction of 0.49 and 0.74, the system can crystallize into a face centered cubic (fcc) structure (Fig. 3B). In the presence of large particles, see Fig. 3C, crystallization is hindered. The large particles, shown in green, completely suppress crystal formation as sketched in Fig. 3D. In contrast, a mixture of small and large compressible microgels, red and green in Fig. 3E, can crystallize in spite of a high polydispersity, as the volume fraction of the suspension is increased. In Fig. 3F, the large and softest microgel particles are compressed to about the size of the small ones to fit in the crystal structure without any point defects. Furthermore, the fcc arrangement is found to be the equilibrium structure as in monodisperse suspensions: Once the larger particles are compressed, the suspension of soft spheres crystallizes as a suspension of monodisperse microgels but with the freezing point shifted to higher concentrations [1, 8].

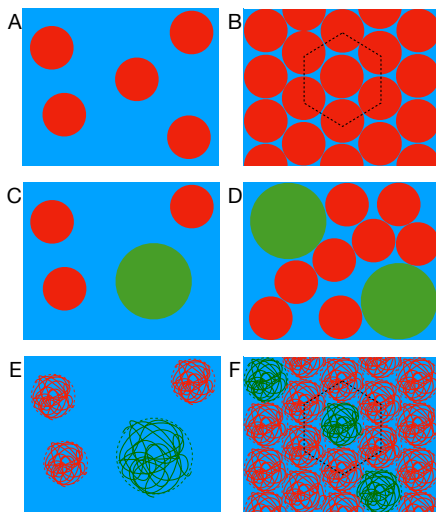


Figure 3

Sketch of the arrangement of small (red) and large (green) spheres at low (left column) and high (right column) concentration. (A)-(D) Hard, incompressible spheres. (E), (F) Soft, compressible, spheres. The dashed black lines in (B) and (F) highlight the crystalline structure.

As explained in this report, SANS with contrast matching is a key method to understand the behavior of colloidal polymer particles such as microgels at high concentrations. Together with measurements of the osmotic pressure of the samples used in the SANS study and with a systematic study of the phase behavior of concentrated suspensions using structure factors obtained with SAXS, we have shown how the osmotic pressure of the suspension and the ratio between the bulk moduli of the particles mixed in the sample are the key parameters of the spontaneous particle deswelling of microgels at high vol-

ume fractions [1]. Moreover, the spontaneous particle deswelling has a profound effect on the phase behavior of the studied pNIPAM microgels. Suspensions with polydispersities expected to totally suppress crystallization are found to crystallize as soon as the selective particle deswelling of the softest and largest microgel particles reduces the polydispersity. The role of polydispersity, therefore, differs in a fundamental way from that in hard spheres, where polydispersity always hinders crystallization or totally suppresses

crystallization for polydispersities above 12% [9–11]. In contrast, we have shown how spontaneous particle deswelling in pNIPAM microgels allows for crystallization up to a polydispersity of 18.5% [8]. As the deswelling mechanism that we have unraveled for the pNIPAM microgels [1] is based on the presence of charges on the surface of compressible particles, we expect the deswelling mechanism to be quite general and to apply for other soft polymer particles.

- [1] A. Scotti, U. Gasser, E. S. Herman, M. Pelaez-Fernandez, L. A. Lyon, and A. Fernandez-Nieves, *Proc. Natl. Acad. Sci. USA* **113**, 5576 (2016).
- [2] U. Gasser, J. Hyatt, J.-J. Lietor-Santos, E. Herman, L. A. Lyon, and A. Fernandez-Nieves, *J. Chem. Phys.* **141** (2014).
- [3] A. S. J. Iyer and L. A. Lyon, *Angew. Chem. Int. Ed.* **48**, 4562 (2009).
- [4] H. Senff and W. Richtering, *J. Chem. Phys.* **111**, 1705 (1999).
- [5] S. Debord and L. A. Lyon, *J. Phys. Chem. B* **107**, 2927 (2003).
- [6] M. Stieger, J. S. Pedersen, P. Lindner, and W. Richtering, *Langmuir* **20**, 7283 (2004).
- [7] A. John, V. Breedveld, and L. A. Lyon, *J. Phys. Chem. B* **111**, 7796 (2007).
- [8] A. Scotti, U. Gasser, E. S. Herman, J. Han, A. Menzel, L. A. Lyon, and A. Fernandez-Nieves, *Phys. Rev. E* **96**, 032609 (2017).
- [9] D. Frenkel, *Nature* **460**, 465 (2009).
- [10] D. Kofke and P. Bolhuis, *Phys. Rev. E* **59**, 618 (1999).
- [11] S. Phan, W. Russel, J. Zhu, and P. Chaikin, *J. of Chem. Phys.* **108**, 9789 (1998).
- [12] W. Blackburn and L. A. Lyon, *Colloid. Polym. Sci.* **286**, 563 (2008).
- [13] M. Andersson and S. L. Maunu, *J. Polym. Sci. :Part B: Polym. Phys.* **44**, 3305 (2006).
- [14] D. E. Koppel, *J. Chem. Phys.* **57**, 4814 (1972).
- [15] A. Scotti, W. Liu, J. S. Hyatt, E. S. Herman, H. S. Choi, J. Kim, L. A. Lyon, U. Gasser, and A. Fernandez-Nieves, *J. Chem. Phys.* **142**, 234905 (2015).
- [16] A. Furrer, J. Mesot, and T. Strässle, in *Neutron Scattering in Condensed Matter Physics* (World Scientific, 2009) Chap. 13.
- [17] G. Batchelor, *J. Fluid Mech.* **83**, 97 (1977).
- [18] M. Stieger, W. Richtering, J. Pedersen, and P. Lindner, *J. Chem. Phys.* **120**, 6197 (2004).
- [19] A. Fernandez-Barbero, A. Fernandez-Nieves, I. Grillo, and E. Lopez-Cabarcos, *Phys. Rev. E* **66**, 051803 (2002).
- [20] P. Pedersen, D. Posselt, and K. Mortensen, *J. Appl. Cryst.* **23**, 321 (1990).
- [21] G. M. Conley, S. Nöjd, M. Braibanti, P. Schurtenberger, and F. Scheffold, *Colloids and Surfaces A: Physicochem. Eng. Aspects* **499**, 18 (2016).
- [22] A. P. H. Gelissen, A. Oppermann, T. Caumanns, P. Hebbeker, S. K. Turnhoff, R. Tiwari, S. Eisold, U. Simon, Y. Lu, J. Mayer, W. Richtering, A. Walther, and D. Wll, *Nano Letters* **16**, 7295 (2016).
- [23] P. S. Mohanty, S. Nöjd, K. v. Griethuysen, J. J. Crassous, M. Obiols-Rabasa, R. Schweins, A. Stradner, and P. Schurtenberger, *Scientific Reports* **7**, 1487 (2017).

Announcements

General Assembly 2017 of SGN

The General Assembly of SGN will take place on November 3rd, 2017, at 17:00 in the main auditorium, WHGA/001, of PSI.

SGN/SSDN Members

Presently the SGN has 212 members. New members can register online on the SGN website: <http://sgn.web.psi.ch>

SGN/SSDN Annual Member Fee

The SGN/SSDN members are kindly asked to pay their annual member fees. At the general assembly 2013 of the society, the fee has been increased from CHF 10 to **CHF 20**. It can be paid either by bank transfer or in cash during your next visit at PSI. The bank account of the society is accessible for both Swiss national and international bank transfers:

Postfinance: 50-70723-6 (BIC: POFICHBE),
IBAN: CH39 0900 0000 5007 0723 6.

The SGN is an organization with tax charitable status. All fees and donations paid to the SGN are **tax deductible**.

PSI Facility News

Recent news and scientific highlights of the three major PSI user facilities SLS, SINQ and SμS can be found in the **quarterly electronic newsletter** available online under: <https://www.psi.ch/science/facility-newsletter>

SINQ Call for Proposals

The next **deadline** for the submission of beam time requests for the Swiss spallation neutron source 'SINQ' (<http://sinq.web.psi.ch>) is:

Feb 20, 2018

Registration of publications

Please remember to **register all publications either based on data taken at SINQ, SLS, SμS or having a PSI co-author** to the Digital User Office: <https://duo.psi.ch>. Please follow the link 'Publications' from your DUO main menu.

Open Positions at SINQ and ILL

To look for open positions at SINQ or ILL, have a look at the following webpages:

<https://www.psi.ch/pa/stellenangebote/>

<https://www.ill.eu/careers/all-our-vacancies/?L=0>

PhD positions at ILL

The PhD program of the Institut Laue-Langevin, ILL, is open to researchers in Switzerland. Consult the page: <https://www.ill.eu/science-technology/phd-students/home/> for information on the PhD program of ILL or get in contact with the managers of the program using the email address phd_rep@ill.eu.

The Swiss agreement with the ILL includes that ILL funds and hosts one PhD student from Switzerland.

Conferences and Workshops 2017 and beyond

An updated list with online links can be found here:
<http://www.psi.ch/useroffice/conference-calendar>

November 2017

62nd Annual Conference on Magnetism and
Magnetic Materials
November 6-10, 2017, Pittsburgh, PA, USA

Neutrons Matter VII
November 7-8, 2017, Rome, Italy

25th Protein Structure Determination in Industry
Meeting, November 12-14, 2017, Cambridge, UK

From Single- to Multiomics: Applications and
Challenges in Data Integration
November 12-14, 2017, Heidelberg, Germany

Macromolecular Crystallography School 2017
November 13-23, 2017, Montevideo, Uruguay

EMBL Conference: Revolutions in Structural
Biology: Celebrating the 100th Anniversary of
Sir John Kendrew
November 16-17, 2017, Heidelberg, Germany

ICEAS2017: International Conference on Ap-
plied Sciences and Engineering 2017
November 16-17, 2017, Tirana, Albania

The 9th AONSA/The 2nd Neutron and Muon
School
November 16-20, 2017, Tokai, Japan

ICG: Italian Crystal Growth
November 20-21, 2017, Milan, Italy

2017 MRS Fall Meeting and Exhibit
November 26 - December 1, 2017, Boston, MA,
USA

ISSX2: In Situ Serial Crystallography Workshop
November 27-29, 2017, Villigen, Switzerland

December 2017

Crystal 31: The 31st Biennial Conference of the Society of Crystallographers in Australia and New Zealand, December 3-7, 2017, Pullman Bunker Bay, Australia

Structural and biophysical methods for biological macromolecules in solution

December 6-14, 2017, Singapore

High-Accuracy CLEM: Applications at Room Temperature and in cryo

December 10-15, 2017, Heidelberg, Germany

9th Joint BER II and BESSY II User Meeting

December 13-15, 2017, Berlin, Germany

3rd International Workshop on Material Science and Chemical Engineering

December 16-17, 2017, Istanbul, Turkey

January 2018

13th SOLEIL Users' Meeting

January 18-19, 2018, Synchrotron Soleil, Palaiseau, France

Rigi-Workshop on Networks and interactions - from species to communities

January 21-23, 2018, Rigi Kulm, Switzerland

February 2018

Cryo-EM from Cells to Molecules: Multi-Scale Visualization of Biological Systems (F1). A Keystone Symposium on Cryo-EM

February 4-8, 2018, Tahoe City, CA, USA

BV49: PSI Particle Physics Users' Meeting 2018, February 12-14, 2018, Villigen, Switzerland

March 2018

38th Berlin School on Neutron Scattering

March 1-9, 2018, Berlin, Germany

26th Annual Meeting of the German Crystallographic Society (DGK)

March 5-8, 2018, Essen, Germany

April 2018

XOPT'18: International Conference on X-ray Optics and Applications 2018

April 24-27, 2018, Yokohama, Japan

IPAC18: International Particle Accelerator Conference 2018

April 29 - May 4, 2018, Vancouver, BC, Canada

May 2018

Fatigue 2018

May 27 - June 1, 2018, Poitiers, France

June 2018

SRI 2018: 13th International Conference on Synchrotron Radiation Instrumentation

June 11-16, 2018, Taipei, Taiwan

14th Bombannes Summer School on Scattering Methods Applied to Soft Condensed Matter

June 19-26, 2018, Bombannes, France

July 2018

SXNS15: 2018 International Conference on Surface X-ray and Neutron Scattering

July 15-19, 2018, Pohang Light Source, Republic of Korea

XAFS2018: 17th International Conference on X-ray Absorption Fine Structure

July 22-27, 2018, Krakow, Poland

Gordon Research Conference Scientific Methods in Cultural Heritage Research

July 22-27, 2018, Castelldefels, Spain

August 2018

HRM2018: 14th International Conference on X-ray Microscopy

August 19-24, 2018, Saskatoon, Saskatchewan, Canada

ECM31: 31st European Crystallographic Meeting

August 22-27, 2018, Oviedo, Spain

7th EuChemS Chemistry Congress

August 26-30, 2018, Liverpool, UK

October 2018

SAS2018: XVII International Conference on Small-Angle Scattering

October 7-12, 2018, Traverse City, MI, USA

Neutrons and Food 2018

October 16-19, 2018, Sydney, Australia

Editorial

Editor

Swiss Neutron Scattering Society

Board for the Period

October 2015 – October 2018:

President

Prof. Dr. Henrik Ronnow
henrik.ronnow@epfl.ch

Board Members

Prof. Dr. M. Kenzelmann
michel.kenzelmann@psi.ch

Dr. L.E. Bove

livia.bove@epfl.ch

PD Dr. U. Gasser (secretary)

urs.gasser@psi.ch

Honorary Members

Prof. Dr. W. Hälg, ETH Zürich (†)

Prof. Dr. K. A. Müller

IBM Rüschlikon and Univ. Zürich

Prof. Dr. A. Furrer

ETH Zürich and Paul Scherrer Institut

Auditors

PD Dr. K. Krämer, University of Berne
Dr. M. Zolliker, Paul Scherrer Institut

Address

Sekretariat SGN/SSDN
c/o Paul Scherrer Institut
WLGA/018
5232 Villigen PSI, Switzerland
phone: +41 56 310 46 66
fax: +41 56 310 32 94
<http://sgn.web.psi.ch>

Bank Account

Postfinance: 50-70723-6 (BIC: POFICHBE)
IBAN: CH39 0900 0000 5007 0723 6

Printing

Paul Scherrer Institut
Circulation: 1600
2 numbers per year

Copyright

SGN/SSDN and the respective authors

Swiss Neutron Scattering Society

Sekretariat SGN/SSDN
WLGA/018
Paul Scherrer Institut
5232 Villigen PSI, Switzerland

